AD-A065 466 ARMY MISSILE RESEARCH AND DEVELOPMENT COMMAND REDSTO--ETC F/G 20/11
STRESS INTENSITIES AROUND SURFACE FLAWS IN CYLINDRICAL SHELLS B--ETC(U)
DEC 78 T L VANDIVER, J SCHAEFFEL, D G SMITH

UNCLASSIFIED DRDMI-T-79-11 NL

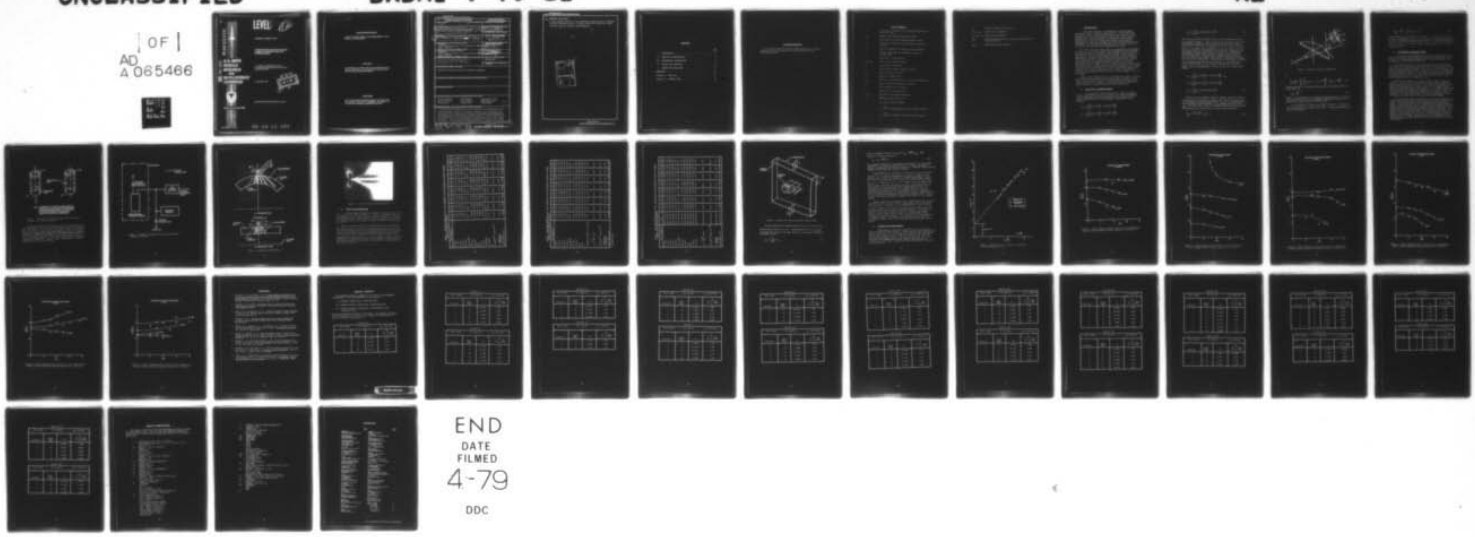

END
DATE
FILMED
4-79
DDC

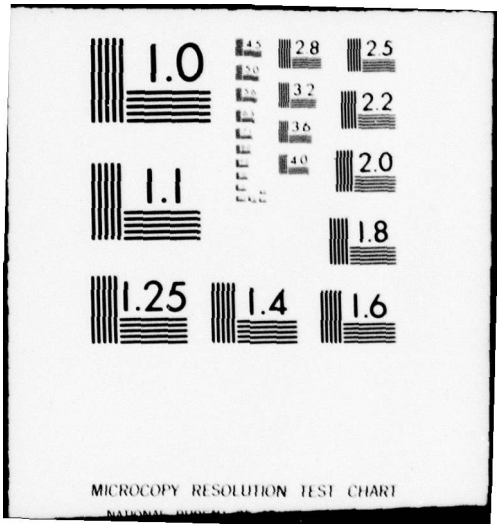
1.0
1.1
1.25
1.4
1.6
2.8
3.2
3.6
4.0
2.5
2.2
2.0
1.8
MICROCOPY RESOLUTION TEST CHART

LEVEL II

AD A065466

DDC FILE COPY

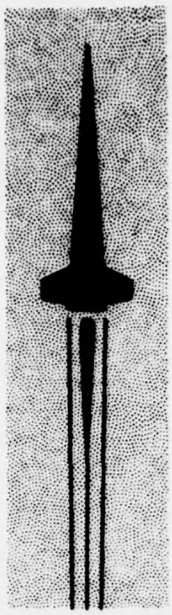

U.S. ARMY MISSILE RESEARCH AND DEVELOPMENT COMMAND

Redstone Arsenal, Alabama 35809

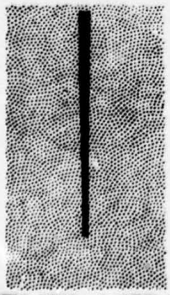

DMI FORM 1000, 1 APR 77

TECHNICAL REPORT T-79-11

STRESS INTENSITIES AROUND SURFACE FLAWS IN CYLINDRICAL SHELLS BY STRESS FREEZING

T. L. Vandiver, J. Schaeffel, and D. G. Smith
Ground Equipment and Missile Structures Directorate
Technology Laboratory

15 December 1978

Approved for public release; distribution unlimited.

79 03 05 031

DISPOSITION INSTRUCTIONS

DESTROY THIS REPORT WHEN IT IS NO LONGER NEEDED. DO NOT RETURN IT TO THE ORIGINATOR.

DISCLAIMER

THE FINDINGS IN THIS REPORT ARE NOT TO BE CONSTRUED AS AN OFFICIAL DEPARTMENT OF THE ARMY POSITION UNLESS SO DESIGNATED BY OTHER AUTHORIZED DOCUMENTS.

TRADE NAMES

USE OF TRADE NAMES OR MANUFACTURERS IN THIS REPORT DOES NOT CONSTITUTE AN OFFICIAL INDORSEMENT OR APPROVAL OF THE USE OF SUCH COMMERCIAL HARDWARE OR SOFTWARE.

UNCLASSIFIED

SECURITY CLASSIFICATION OF THIS PAGE *(When Data Entered)*

REPORT DOCUMENTATION PAGE

READ INSTRUCTIONS BEFORE COMPLETING FORM

1. REPORT NUMBER: T-79-11
2. GOVT ACCESSION NO.
3. RECIPIENT'S CATALOG NUMBER

4. TITLE (and Subtitle): STRESS INTENSITIES AROUND SURFACE FLAWS IN CYLINDRICAL SHELLS BY STRESS FREEZING
5. TYPE OF REPORT & PERIOD COVERED: Technical Report
6. PERFORMING ORG. REPORT NUMBER

7. AUTHOR(s): T. L. Vandiver, J. Schaeffel [redacted] D. G. Smith
8. CONTRACT OR GRANT NUMBER(s): 45p.

9. PERFORMING ORGANIZATION NAME AND ADDRESS
Commander
US Army Missile Research and Development Command
ATTN: DRDMI-TLA
Redstone Arsenal, Alabama 35809

10. PROGRAM ELEMENT, PROJECT, TASK AREA & WORK UNIT NUMBERS: DA ILI62303A214

11. CONTROLLING OFFICE NAME AND ADDRESS
Commander
US Army Missile Research and Development Command
ATTN: DRDMI-TI
Redstone Arsenal, Alabama 35809

12. REPORT DATE: 15 December 1978
13. NUMBER OF PAGES: 42

14. MONITORING AGENCY NAME & ADDRESS *(if different from Controlling Office)*: DRDMI-T-79-11
15. SECURITY CLASS. *(of this report)*: UNCLASSIFIED
15a. DECLASSIFICATION/DOWNGRADING SCHEDULE

16. DISTRIBUTION STATEMENT *(of this Report)*

Approved for public release; distribution unlimited.

17. DISTRIBUTION STATEMENT *(of the abstract entered in Block 20, if different from Report)*

18. SUPPLEMENTARY NOTES

19. KEY WORDS *(Continue on reverse side if necessary and identify by block number)*

Stress intensity	Isochromatic	Longitudinal crack
Stress freezing	Part circular	Transverse crack
Photoelastic	Fringe order	Birefringent

20. ABSTRACT *(Continue on reverse side if necessary and identify by block number)*

This report documents a set of 24 tests for the determination of K_I stress intensity factors for isotropic cylinders with longitudinal and transverse part-circular cracks. Part-circular cracks were machined into birefringent Hysol CP5 4290 photoelastic cylinders. The cylinders were then subjected to a stress freezing cycle while under one of two loading conditions: internal pressurization or extension. Slices of the cracks were made at various angles and analyzed with a photoelastic polariscope.

→ next page

DD FORM 1 JAN 73 1473 EDITION OF 1 NOV 65 IS OBSOLETE

UNCLASSIFIED

SECURITY CLASSIFICATION OF THIS PAGE *(When Data Entered)*

393 427 Gm 79 03 06 031

20. ABSTRACT (Continued).

A least-squares curve fit of the photoelastic data was used to generate K_I stress intensity factors. K_I data are plotted versus slice angle into the crack for various crack parameters.

Sub I

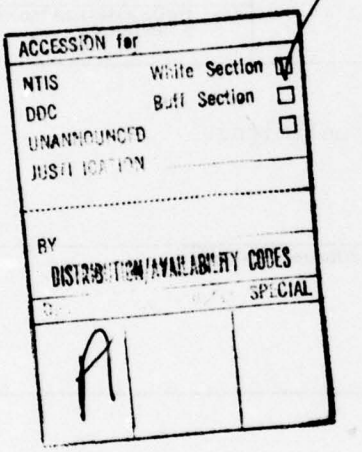

CONTENTS

ACKNOWLEDGEMENTS

The authors sincerely thank Mr. Edward Murphree, Ms. Deborah Russell, and Mr. Steve Swinson for their assistance in this experimental effort.

LIST OF SYMBOLS

A	Crack depth at deepest point (semi-minor diameter for elliptical flaw)
A_c	Nominal cross-sectional area of cylinder
a	Half-length of crack on outside surface of wall
$\bar{D}$	Distance from center of circular flaw to surface of the wall
D	Ratio of distance $\bar{D}$ to radius of circular flaw R
d	Distance from center of cylinder to center of circular flaw
f	Photoelastic fringe constant
K_I, S_{IF}	Mode I stress intensity factor
N	Isochromatic fringe order
P	Total load on cylinder loaded in tension
P_i	Internal cylinder pressure
R	Radius of circular flaw
R_c	Radius of cylinder measured to center of cylinder wall
r, ψ	Polar coordinates centered at crack tip
T	Wall thickness of the cylinder
t	Thickness of a slice analyzed
y, n, θ	Coordinate system shown in Figure 1
σ_m	Nominal cylinder-wall stress
	$\sigma_m = \frac{P}{A_c}$ for tension loading
	$\sigma_m = \frac{P_i R_c}{T}$ for longitudinal flaw and internal pressure
	$\sigma_m = \frac{P_i R_c}{2T}$ for transverse flaw and internal pressure

σ_{on}	Uniform stress at the crack tip
σ_y, σ_n, σ_θ	Normal stress components
τ_{ny}, $\tau_{n\theta}$, $\tau_{y\theta}$	Shear stress components
τ_{max}	Maximum shearing stress in the plane perpendicular to the crack border
θ_{max}	Maximum flaw angle (Figure 6)

I. INTRODUCTION

This work represents a continuation of an effort begun considerably earlier by Mullinix and Smith [1]. That report dealt with surface flaws in hollow cylinders which were subjected to beam bending action. The present work also deals with surface flaws in cylinders, but here the cylinders are subjected to two additional loading cases: uniaxial extension and internal pressurization. Additionally for the latter loading, two surface flaw orientations are considered: the flaw oriented transverse to the cylinder axis as in [1] and the flaw oriented in the longitudinal direction.

As noted in [1], the surface flaw is of considerable technological interest. It has caused a number of well-documented service failures. These failures can be catastrophic and, depending on the severity of the flaw, can occur at a fairly low stress level. This situation is aggravated by the ever-present demand for lighter weight structures, particularly in missile, rocket, and aircraft applications. Because of its importance, the surface flaw was the subject of a special symposium at the 1972 annual meeting of the American Society of Mechanical Engineers (ASME) [2]. A collection of surface flaw solutions was included in the fracture handbook by Smith and Mullinix [3] as well as in the report by Paramerter [4]. Still, insufficient surface flaw solutions exist, and experimental efforts to obtain solutions for specific cases continue; as in the recent article by Smith, et al. [5], for example.

Surface flaws normally occur in a semi-elliptical shape. In order to cut flaws in the cylinders with circular saws, the flaws in this report are represented as part of a circle penetrating various depths into the walls of the cylinders. There appear to be no significant errors involved in using these particular flaw geometries.

II. ANALYTICAL CONSIDERATIONS

The equations of the stresses near the edge of a surface flaw are now well known [6,7,8]. In fact, in a plane perpendicular to the crackfront, the stress distribution near the part-circular crack, corresponding to the opening mode of deformation, can be taken as

$$\sigma_n = \frac{K_I}{(2\pi r)^{1/2}} \cos\frac{\psi}{2}\left(1 - \sin\frac{\psi}{2}\sin\frac{3\psi}{2}\right)$$

$$\sigma_y = \frac{K_I}{(2\pi r)^{1/2}} \cos\frac{\psi}{2}\left(1 + \sin\frac{\psi}{2}\sin\frac{3\psi}{2}\right)$$

$$\tau_{ny} = \frac{K_I}{(2\pi r)^{1/2}} \sin\frac{\psi}{2} \cos\frac{\psi}{2} \cos\frac{3\psi}{2} \quad , \tag{1}$$

where K_I is the stress intensity factor and the coordinates r and ψ are as shown in Figure 1. Thus, the effect on the stress field of the crack border curvature as well as the location and shape of other boundaries is reflected in the magnitude of K_I, the stress intensity factor. The stresses given by Equation (1) are valid only very near the crack tip where it is assumed that the stresses singular in r are much larger than other terms which are regular in r. Experimental measurements, however, must be made at a finite distance from the crack tip where other terms may make a significant contribution to the total stress field. These other terms must somehow be accounted for if K_I is to be determined. A simple way of approximately accounting for the regular terms was provided by Irwin [9]. Irwin assumed a uniform stress field, σ_{on}, at the crack tip parallel to the crack plane. With this superposition, the form of the local stress field becomes

$$\sigma_n = \frac{K_I}{(2\pi r)^{1/2}} \cos\frac{\psi}{2}\left(1 - \sin\frac{\psi}{2}\sin\frac{3\psi}{2}\right) - \sigma_{on}$$

$$\sigma_y = \frac{K_I}{(2\pi r)^{1/2}} \cos\frac{\psi}{2}\left(1 + \sin\frac{\psi}{2}\sin\frac{3\psi}{2}\right)$$

$$\tau_{ny} = \frac{K_I}{(2\pi r)^{1/2}} \sin\frac{\psi}{2} \cos\frac{\psi}{2} \cos\frac{3\psi}{2} \tag{2}$$

While σ_{on} has no influence upon the singular stress field itself, it does alter the isochromatic fringe pattern, which is proportional to the maximum in-plane stearing stress. In the use of photoelasticity, the most readily obtained quantity is the maximum shearing stress, τ_{max}. From this stress field, the maximum shearing stress in the plane perpendicular to the crack front, y-n, can be determined from

$$\tau_{max}^2 = \frac{(\sigma_n - \sigma_y)^2}{2} + \tau_{ny}^2 \quad , \tag{3}$$

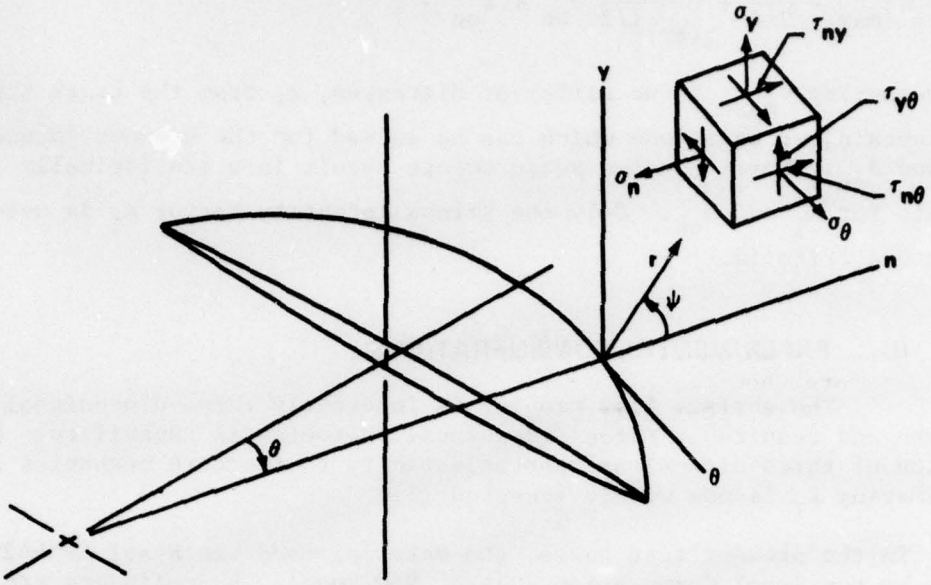

Figure 1. Sketch of crack tip coordinates.

as

$$\left(2\tau_{max}\right)^2 = \left[\frac{K_I}{(2\pi r)^{1/2}} \sin\psi + \sigma_{on} \sin\frac{3\psi}{2}\right]^2 + \left(\sigma_{on} \cos\frac{3\psi}{2}\right)^2 \quad . \quad (4)$$

Photoelastically, the maximum shearing stress is determined from the stress optic law

$$\tau_{max} = \frac{fN}{2t} \quad , \quad (5)$$

where t is the thickness of the specimen measured parallel to the direction of the light, N is the isochromatic fringe order, and f is the photoelastic fringe constant for the material.

It is convenient to measure τ_{max} along the line $\psi = \pi/2$ where the maximum shearing stress is known to be large. Simplifying Equation (4) at $\psi = \pi/2$ results in

$$4\tau_{max}^2 = \frac{K_I^2}{2\pi r} + \frac{K_I}{(\pi r)^{1/2}} \sigma_{on} + \sigma_{on}^2 \quad . \tag{6}$$

By measuring τ_{max} at two different distances, r, from the crack tip, one can obtain two equations which can be solved for the unknown parameters K_I and σ_{on}. More than two measurements result in a statistically improved result for K_I and σ_{on}. Only the stress intensity factor K_I is used in fracture criteria.

III. EXPERIMENTAL CONSIDERATIONS

The surface flaw problem is inherently three-dimensional in nature and requires a three-dimensional photoelastic capability. Application of three-dimensional photoelasticity to fracture mechanics for estimating K_I is now widely accepted [5].

In the present test cases, the material used was Hysol CP5-4290 cast by the Hysol Corporation, Olean, New York. The cylinders are nominally 5.875 in. in outside diameter with a 0.75-in. wall thickness. Two specimen configurations were used: one with the surface flaw transverse to the cylinder axis and one with the flaw oriented in the longitudinal direction as shown in Figure 2. The flaws were machined with a circular saw blade 0.006-in. thick. Blade radii of 0.875 and 1.500 in. were used to produce flaws of two different sizes.

As indicated in Figure 2, a total of three series of tests were conducted: a series for the transversely-flawed cylinder loaded in uniform uniaxial tension, a series for the transversely-flawed cylinder loaded with internal pressure, and a series for the longitudinally-flawed cylinder loaded with internal pressure. The uniform tension load was applied simply by hanging dead weights on the cylinder. The internal pressure load was supplied by compressed air passing through a regulator. The pressure was measured by a Mercury manometer. Figure 3 is a schematic of the setup for the internal pressure loading.

After the surface flaw was machined, the cylinder was annealed by thermal soaking at 280°F for 6 hours followed by cooling at the rate of 1°F/hr. The stress freezing of the loaded models was accomplished using the same thermal cycle as for annealing except under loading conditions. After the stress freezing cycle, slices perpendicular to the crack border were removed from the model by means of a band saw. Figure 4 shows a few of the various angles at which slices were taken. The number of slices varied from test to test depending upon the flaw size. Each slice was polished with sand paper. The CP5-4290 material was calibrated for its fringe constant by means of a beam loaded in pure bending using dead weights and subject to the same thermal cycle as for the cylinders.

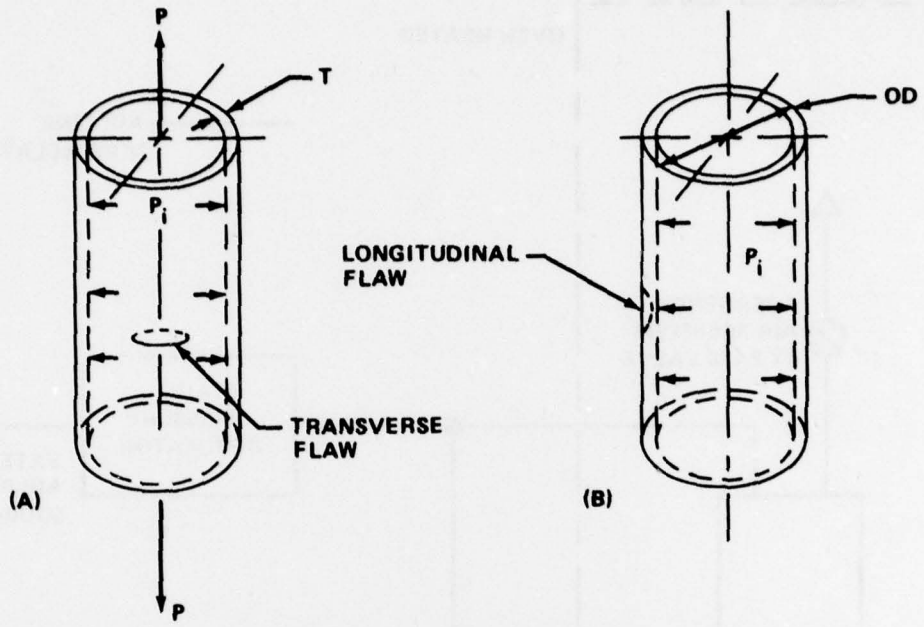

NOTE: *TRANSVERSELY–FLAWED CYLINDER SUBJECTED SEPARATELY TO BOTH UNIAXIAL EXTENSION AND INTERNAL PRESSURE LOADING. THE CYLINDERS WITH INTERNAL PRESSURE LOADING WERE SUBJECT TO FIXED END–CAP CONDITIONS.*

Figure 2. Transverse (A) and longitudinal (B) flaw loading geometry for a hollow cylinder.

To improve resolution for analysis, slices were placed in an oil bath consisting of 75.5% by volume of Halowax oil and 24.5% mineral oil. The index of refraction of the oil was the same as the CP5-4290 material; therefore, light scatter was minimized. The slices were observed in a comparator polariscope at 10X magnification. By means of an x-y table on the polariscope, points on the slices could be located to within ±0.0001 in. Fractional fringe orders were obtained using Tardy compensation. Figure 5 shows a photograph of a typical fringe pattern at a slice crack tip.

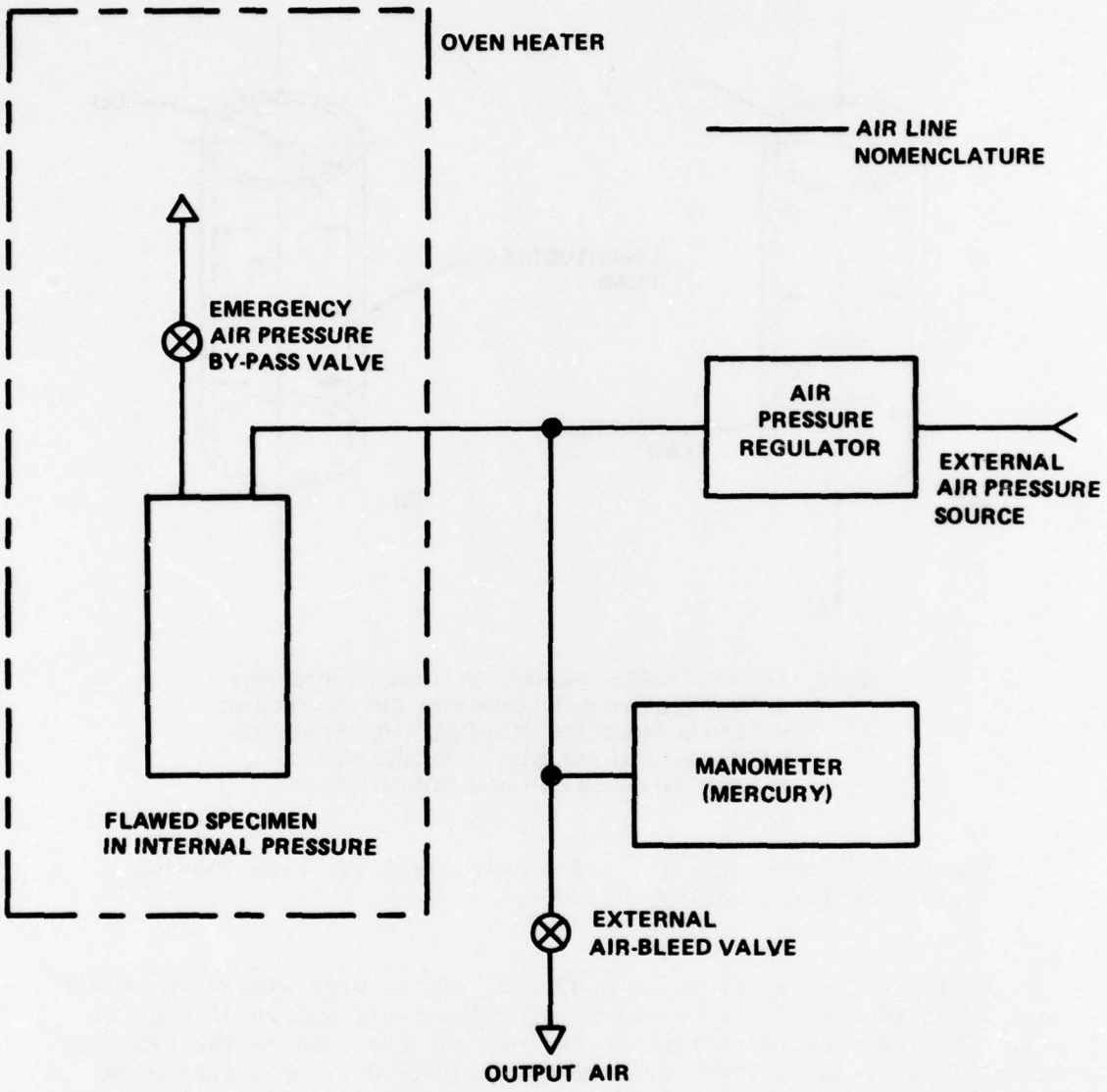

Figure 3. Schematic configuration for internal pressure loading of cylinders.

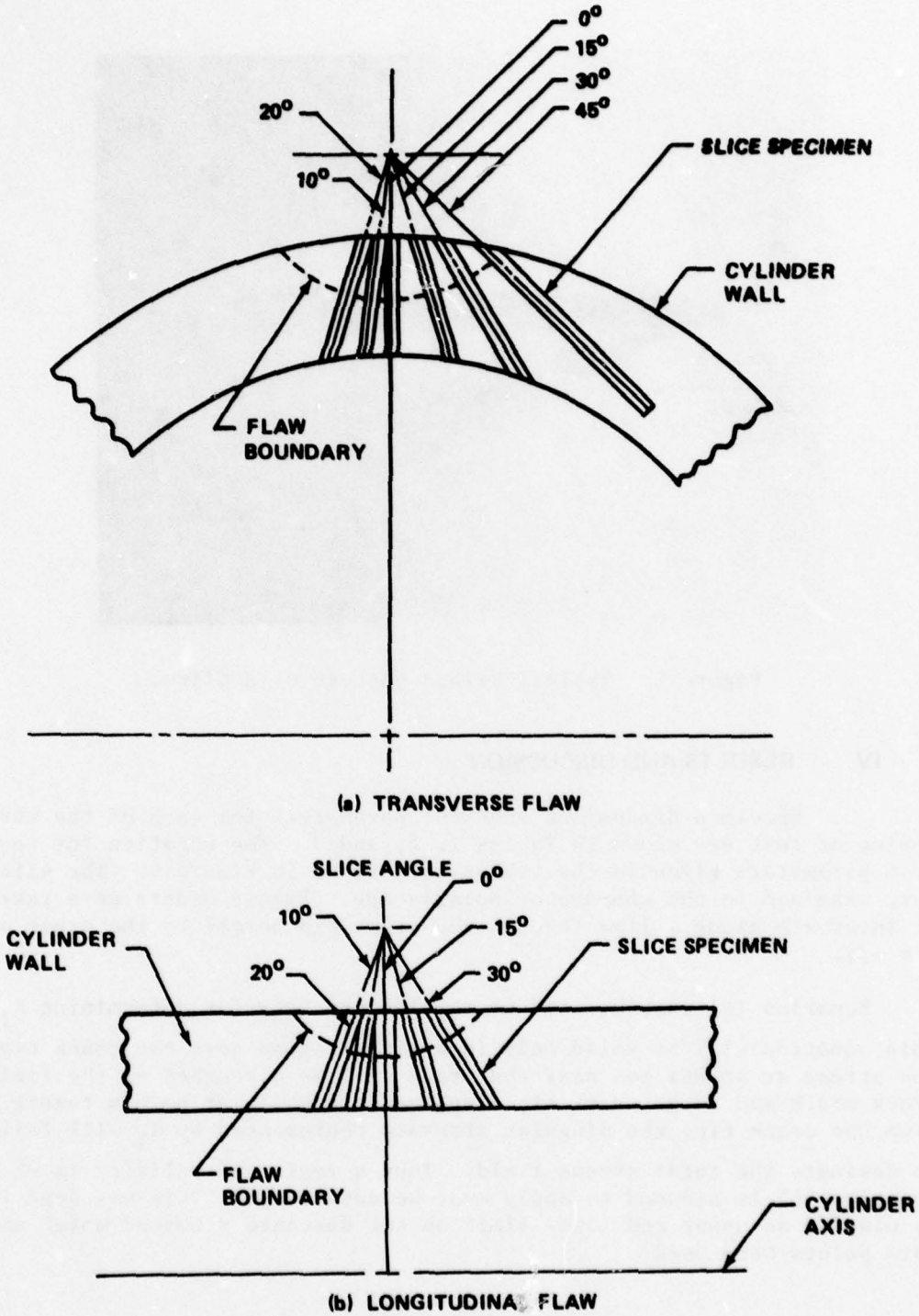

Figure 4. Example slicing schemes.

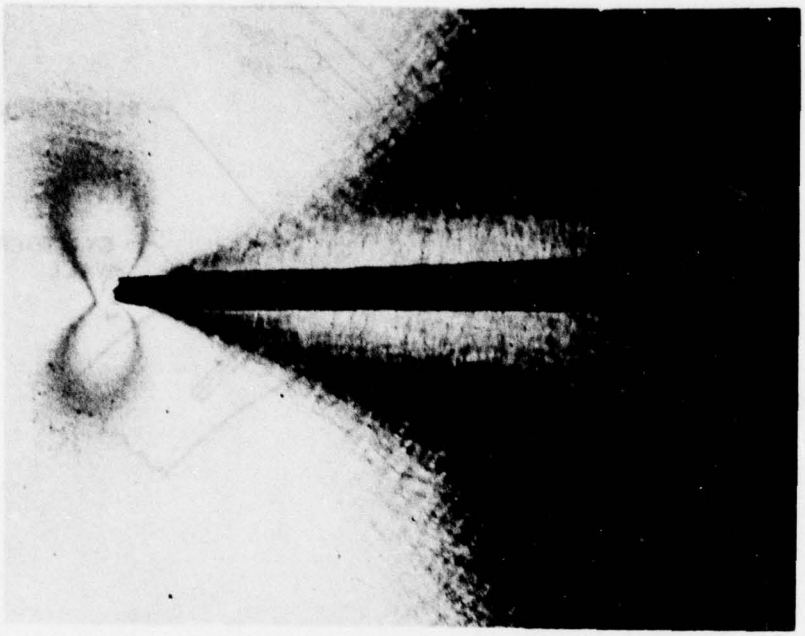

Figure 5. Typical fringe pattern of a slice.

IV. RESULTS AND DISCUSSION

Specimen dimensions and test parameters for each of the three series of test are shown in Tables 1, 2, and 3. The notation for the test parameters given in the tables is defined in Figure 6. The slices were examined in the comparator polariscope. Fringe orders were taken at intervals along a line through the crack tip normal to the crack at $\psi = \pi/2$.

Equation (6) must be used to resolve the data for determining K_I. This equation will be valid only in a given region near the crack tip. The stress at points too near the crack will be disturbed by the finite crack width and large crack tip displacements while at points remote from the crack tip, the singular stresses represented by K_I will fail to dominate the total stress field. Thus a region of validity in which Equation (6) is assumed to apply must be determined. This was done [1] by placing an upper and lower limit on the distance r beyond which no data points were used.

TABLE 1. SPECIMEN DIMENSIONS AND TEST PARAMETERS FOR TRANSVERSELY-FLAWED CYLINDER LOADED IN UNIAXIAL TENSION

Test Parameters	1T	2T	3T	4T	5T	6T	7T	8T
R (in.)	0.88	0.88	0.88	0.88	1.50	1.50	1.50	1.50
T (in.)	0.706	0.724	0.740	0.721	0.721	0.739	0.718	0.725
A (in.)	0.145	0.282	0.408	0.486	0.145	0.318	0.498	0.800
$\overline{D}$ (in.)	0.729	0.593	0.467	0.389	1.355	1.182	1.002	0.700
OD (in.)	5.88	5.86	5.86	5.86	5.86	5.87	5.90	5.86
θ_{max} (deg)	29.5	41.8	51.2	56.6	21.0	30.9	39.3	51.1
2a (in.)	0.865	1.175	1.376	1.480	1.080	1.560	1.935	2.400
D (in.)	0.834	0.678	0.534	0.444	0.903	0.788	0.668	0.467
A/T	0.206	0.390	0.551	0.674	0.201	0.430	0.693	1.100
a/2a	0.168	0.240	0.296	0.328	0.134	0.204	0.257	0.333
d (in)	3.670	3.523	3.397	3.319	4.280	4.112	3.930	3.630
Load (lb)	125.33	120.03	112.38	115.03	110.38	100.06	94.34	60.37
σ_m (psi)	10.74	10.32	9.72	9.84	9.48	8.42	8.13	5.16
$\frac{2}{\pi}\sigma_m(\pi R)^{1/2}$ (psi-in.$^{1/2}$)	11.34	10.90	10.26	10.39	13.12	11.63	11.24	7.14
f $\left(\frac{\text{psi-in.}}{\text{fringe}}\right)$	1.56	1.56	1.56	1.56	1.56	1.56	1.56	1.56
Crack Width (in.)	0.0082	0.0076	0.0082	0.0080	0.0060	0.0062	0.0065	0.0066

TABLE 2. SPECIMEN DIMENSIONS AND TEST PARAMETERS FOR LONGITUDINAL-FLAWED CYLINDER LOADED WITH INTERNAL PRESSURE

Test Parameters	1PL	2PL	3PL	4PL	5PL	6PL	7PL	8PL
R (in.)	0.875	0.875	0.875	0.875	1.500	1.500	1.500	1.500
T (in.)	0.724	0.727	0.724	0.726	0.728	0.726	0.726	0.733
A (in.)	0.151	0.282	0.400	0.490	0.147	0.325	0.580	0.636
$\overline{D}$ (in.)	0.724	0.593	0.475	0.386	1.353	1.175	0.920	0.864
OD (in.)	5.90	5.90*	5.90*	5.90*	5.88	5.87	5.86	5.89
θ_{max}(deg)	34.16	47.33	57.12	63.82	25.58	38.43	52.17	54.83
2a (in.)	0.98	1.29	1.47	1.57	1.30	1.86	2.37	2.45
D (in.)	0.827	0.678	0.543	0.441	0.902	0.783	0.613	0.576
A/T	0.209	0.388	0.553	0.674	0.202	0.448	0.580	0.868
A/2a	0.154	0.219	0.272	0.312	0.113	0.175	0.245	0.260
d	3.68	3.54	3.42	3.34	4.29	4.11	3.85	3.81
Internal pressure, P_i (psi)	3.67	3.34	2.96	2.70	2.96	2.68	2.28	1.96
$\sigma_m = \frac{P_i R_c}{T}$ (psi)	13.14	11.90	10.59	9.63	10.47	9.49	8.06	6.91
$\frac{2}{\pi}\sigma_m(\pi R)^{1/2}$ (psi-in.$^{1/2}$)	13.88	12.57	11.17	10.16	14.47	13.12	11.14	9.55
f $\left(\frac{\text{psi-in.}}{\text{fringe}}\right)$	1.56	1.56	1.56	1.56	1.56	1.56	1.56	1.56
Crack Width (in.)	0.0094	0.0074	0.0075	0.0090	0.0067	0.0096	0.0078	0.0070

*Assumed value.

TABLE 3. SPECIMEN DIMENSIONS AND TEST PARAMETERS FOR TRANSVERSELY-FLAWED CYLINDER LOADED WITH INTERNAL PRESSURE

Test Parameters	1PC	2PC	3PC	4PC	5PC	6PC	7PC	8PC
R (in.)	Test Failure	0.875	0.875	0.875	1.500	1.500	1.500	1.500
T (in.)	Test Failure	0.721	0.726	0.724	0.718	0.720	0.718	0.710
A (in.)	Test Failure	0.279	0.385	0.488	0.144	0.319	0.491	0.668
$\overline{D}$ (in.)	Test Failure	0.596	0.490	0.387	1.356	1.181	1.009	0.832
OD (in.)	Test Failure	5.86	5.86	5.86	5.86	5.86	5.86	5.86
θ_{max} (deg)	Test Failure	41.63	49.52	56.73	20.61	31.05	39.04	45.91
2a (in.)	Test Failure	1.17	1.34	1.46	1.06	1.55	1.89	2.18
D (in.)	Test Failure	0.681	0.560	0.442	0.904	0.787	0.673	0.555
A/T	Test Failure	0.388	0.531	0.674	0.200	0.443	0.684	0.940
A/2a	Test Failure	0.238	0.287	0.334	0.136	0.205	0.260	0.306
d (in.)	Test Failure	3.526	3.421	3.317	4.286	4.111	3.939	3.762
P_i (psi)	Test Failure	3.33	2.98	5.59	6.22	5.56	4.85	4.16
$\sigma_m = \frac{P_i R_c}{2T}$ (psi)	Test Failure	5.93	5.27	9.91	11.13	9.92	8.68	7.54
$\frac{2}{\pi} \sigma_m (\pi R)^{1/2}$ (psi-in.$^{1/2}$)	Test Failure	6.26	5.56	10.46	15.39	13.71	11.99	10.43
f $\frac{\text{psi-in.}}{\text{fringe}}$	Test Failure	1.56	1.56	1.56	1.56	1.56	1.56	1.56
Crack Width (in.)	Test Failure	0.0058	0.0068	0.0074	0.0079	0.0071	0.0078	0.0091

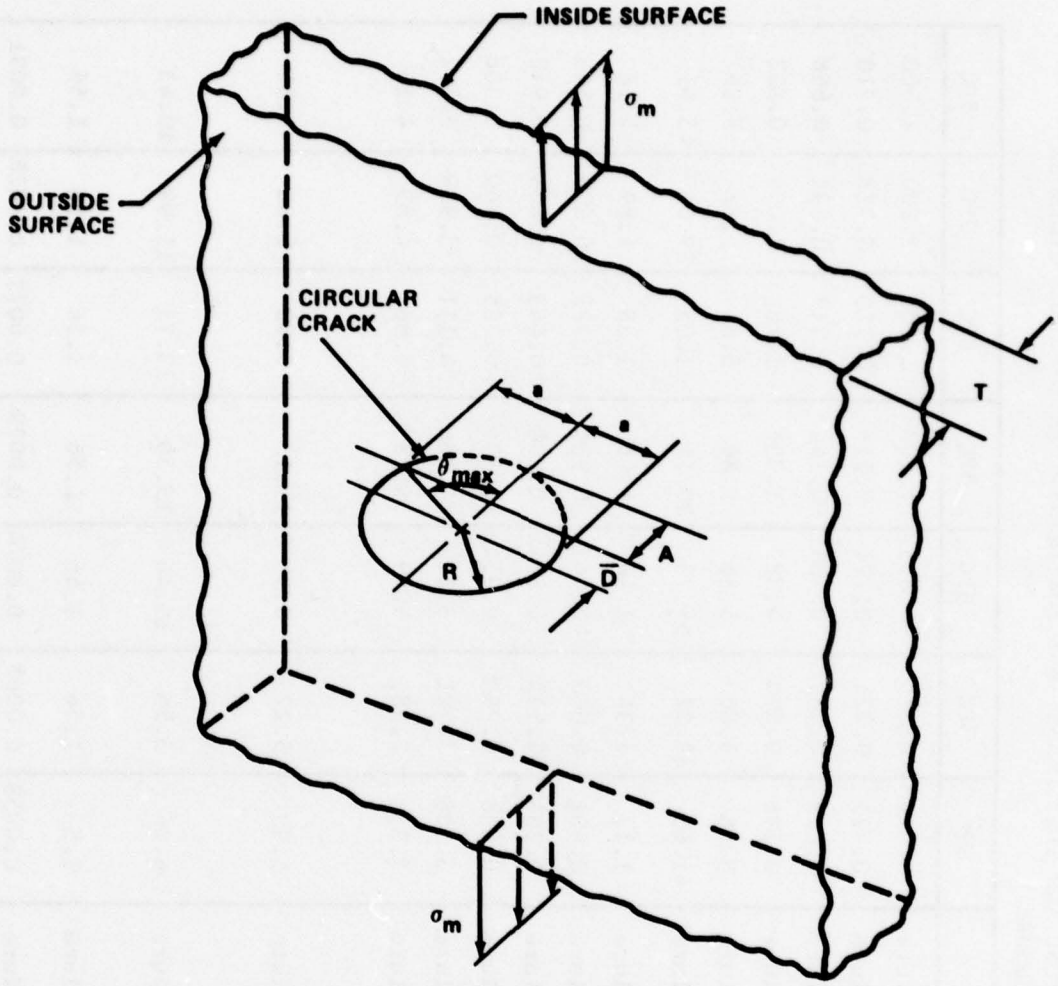

Figure 6. Notation for the part-circular surface flaw.

The approach here will depart from that in [1], in favor of the method used by Smith et al. [5]. Solving Equation (6) for τ_{max} and truncating the results to the same order in r as Equation (2) leads to the simple result:

$$\tau_{max} = \frac{K_I}{\sqrt{8\pi r}} + \sigma_{on} \quad . \tag{7}$$

Define an apparent value of K, K_{ap}, as, $K_{ap} = \sqrt{8\pi r}\ \tau_{max}$. Then Equation (7) can be written as

$$K_{ap} = K_I + \sqrt{8\pi r}\ \sigma_{on} \quad . \tag{8}$$

This equation shows that in the region of valid data, i.e., the region dominated by the singular stresses, there is a linear relationship between the apparent K and the square root of r. Departure from linearity indicates data outside the region of validity.

In determining K_I for a given slice the values of K_{ap} are plotted versus $r^{1/2}$. Data points approximately yielding a straight line are selected and all others are rejected. A least-squares curve is then fit to the selected points and the value of K_I is determined by taking K_{ap} at r = 0, since $K_{ap} = K_I$ at r = 0. Figure 7 gives an example for a typical slice. When the same points are used, this method yields the same results as the statistically more complex method of [1]. The advantage of the present method is its simplicity and the ease of selecting data representative of the singular stresses. Appendix B contains a sample listing of the program used to analyze photoelasticity data on a PDP 11/40 minicomputer with an RT11 software system. Tables 1, 2, and 3 and Figures 8 through 13 summarize the results of the testing program.

Figures 8 and 9 give the results for circumferential flaws in extension for R = 0.875 in. and 1.500 in., respectively. As the A/T aspect ratio increases, an increase in the nondimensional K_I factor for all θ is noted. Figures 10 and 11 give the same general results except that the data appear to have greater experimental scatter. The results of Test 2PL are not shown in Figure 10 due to excessive data scatter. Figures 12 and 13 show similar results for circumferential flawed cylinders with internal pressure. Test 1PC data are not presented due to cylinder failure. The results are generally good for Tests 2PC through 5PC; however, Tests 6PC through 8PC show a great deal of data scatter.

V. SUMMARY AND CONCLUSIONS

Photoelasticity tests were conducted on 24 surface-flawed hollow cylinder specimens loaded in extension and internal pressurization. Results from these tests are presented for transverse and longitudinal semi-circular flawed cylinders having two different flaw radii and several A/T penetration ratios. The tests indicate that for a fixed flaw radii the nondimensional stress intensity increases with an increase in the A/T ratio. Results for these tests coincide in general with those of [1].

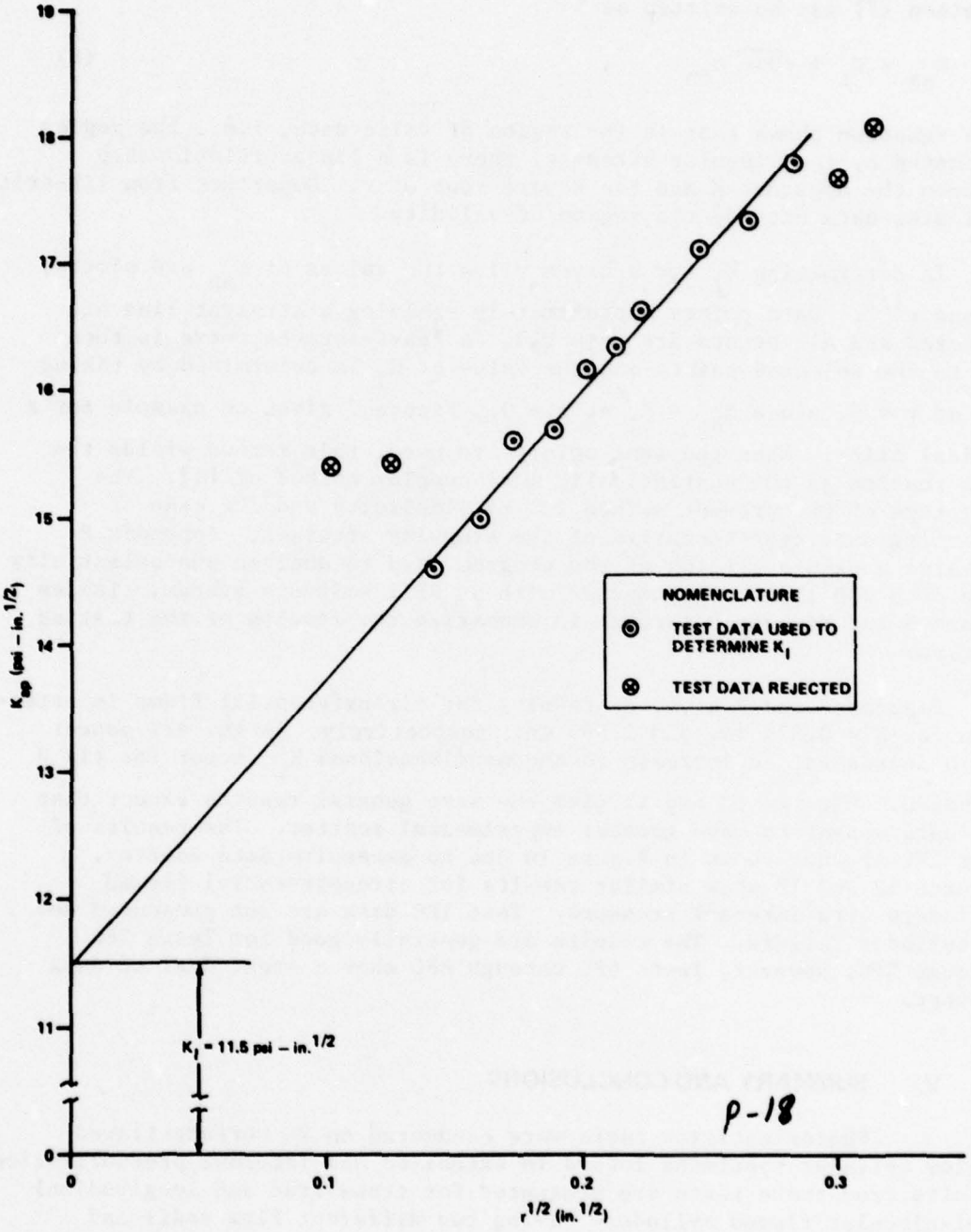

Figure 7. Typical set of slice data, illustrating the determination of K_I.

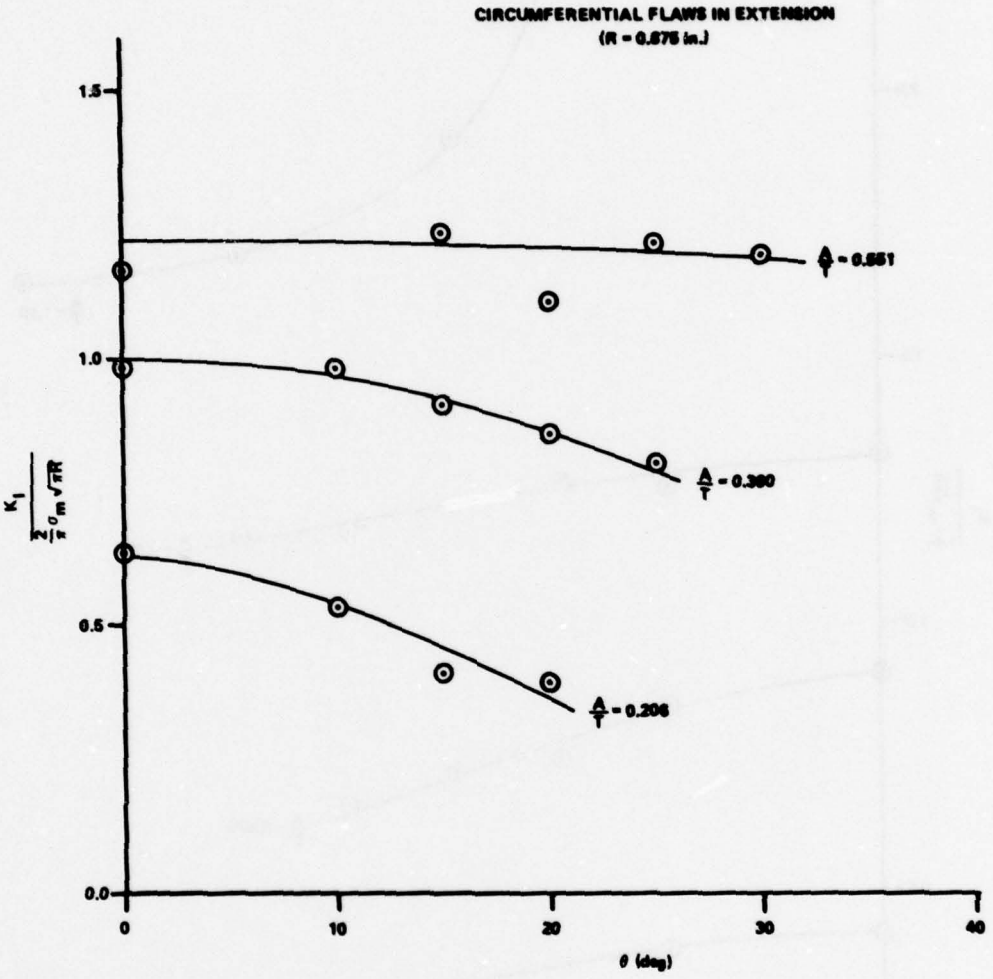

Figure 8. Stress intensity factor versus θ for the transversely-flawed cylinder loaded in uniaxial tension (R = 0.875 in.).

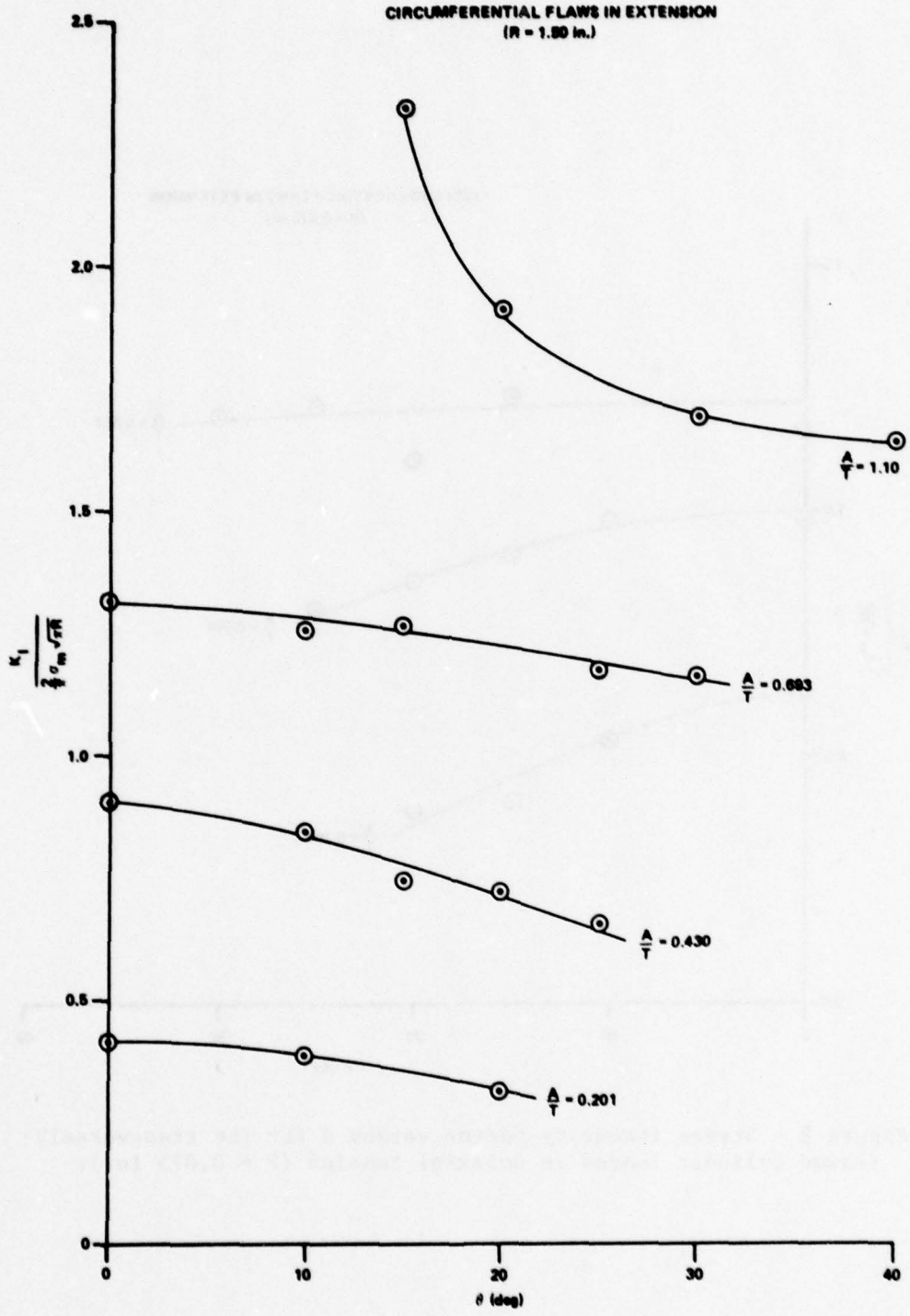

Figure 9. Stress intensity factor versus θ for the transversely-flawed cylinder loaded in uniaxial tension (R = 1.50 in.).

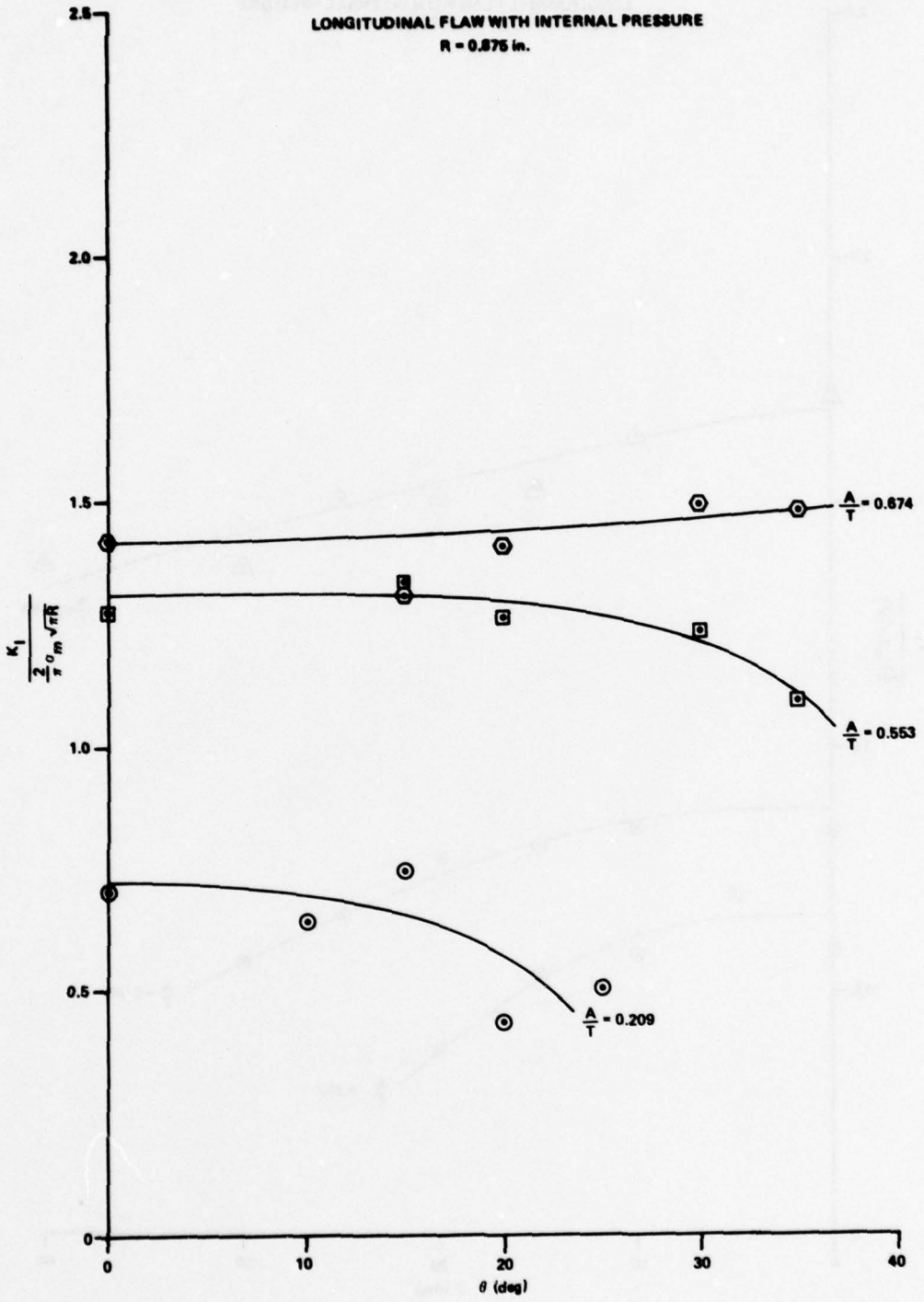

Figure 10. Stress intensity factor versus θ for the longitudinal-flawed cylinder loaded with internal pressure (R = 0.875 in.).

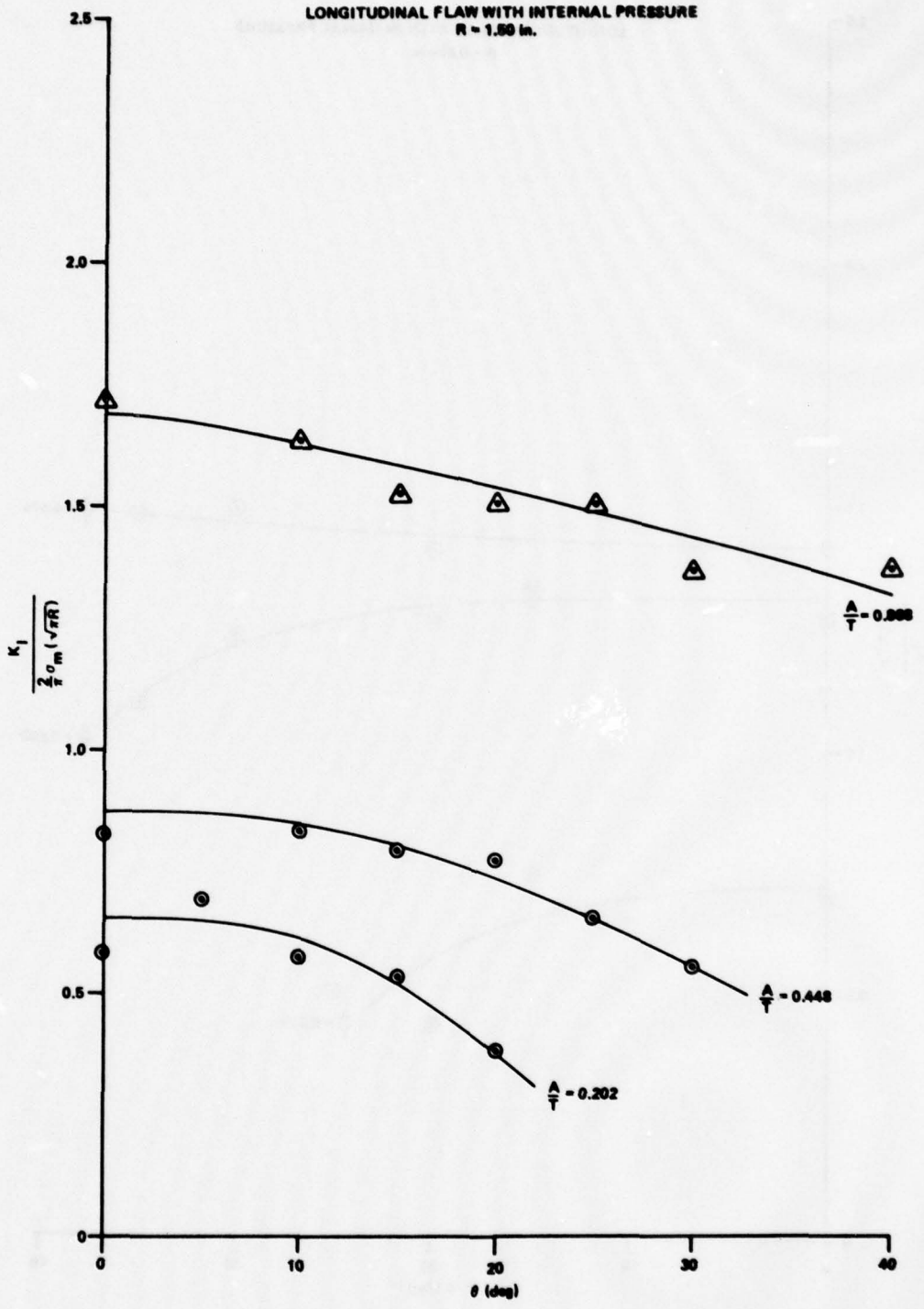

Figure 11. Stress intensity factor versus θ for the longitudinal-flawed cylinder loaded with internal pressure (R = 1.50 in.).

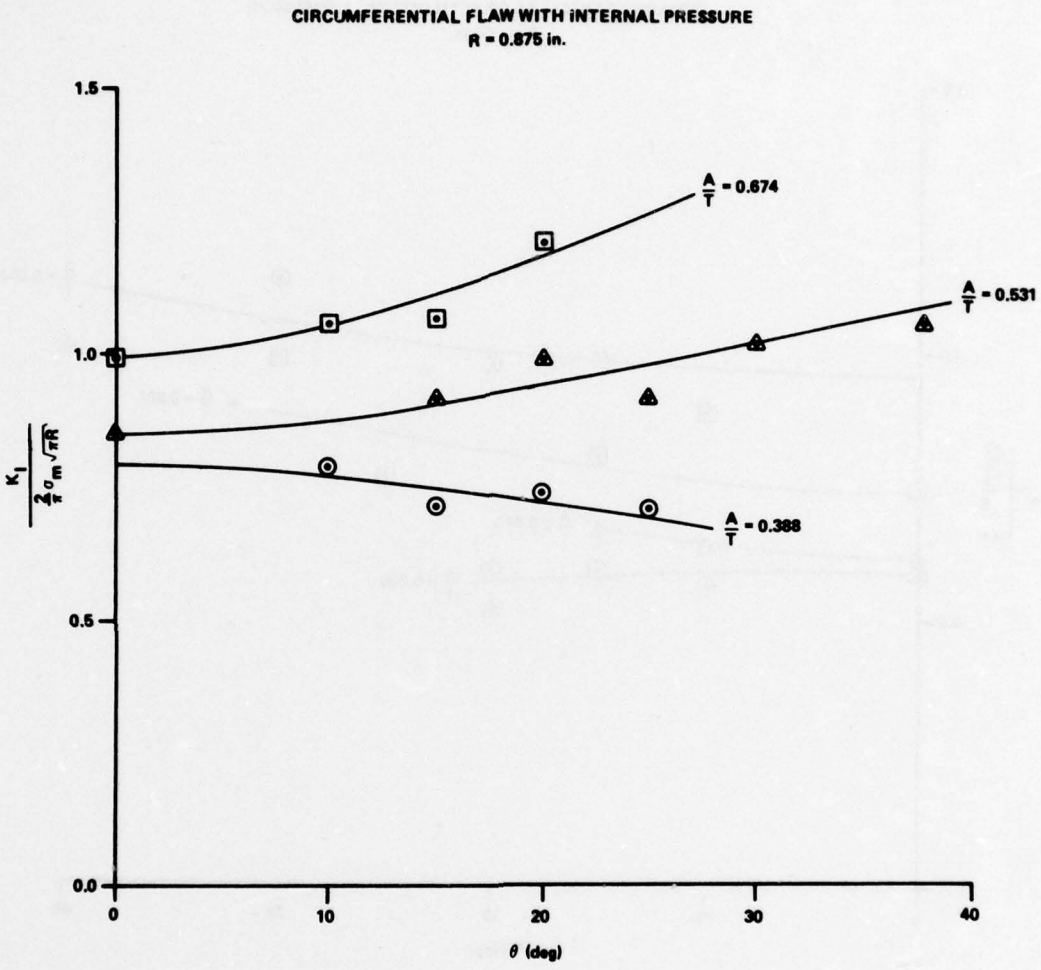

Figure 12. Stress intensity factor versus θ for the transversely-flawed cylinder loaded with internal pressure (R = 0.875 in.).

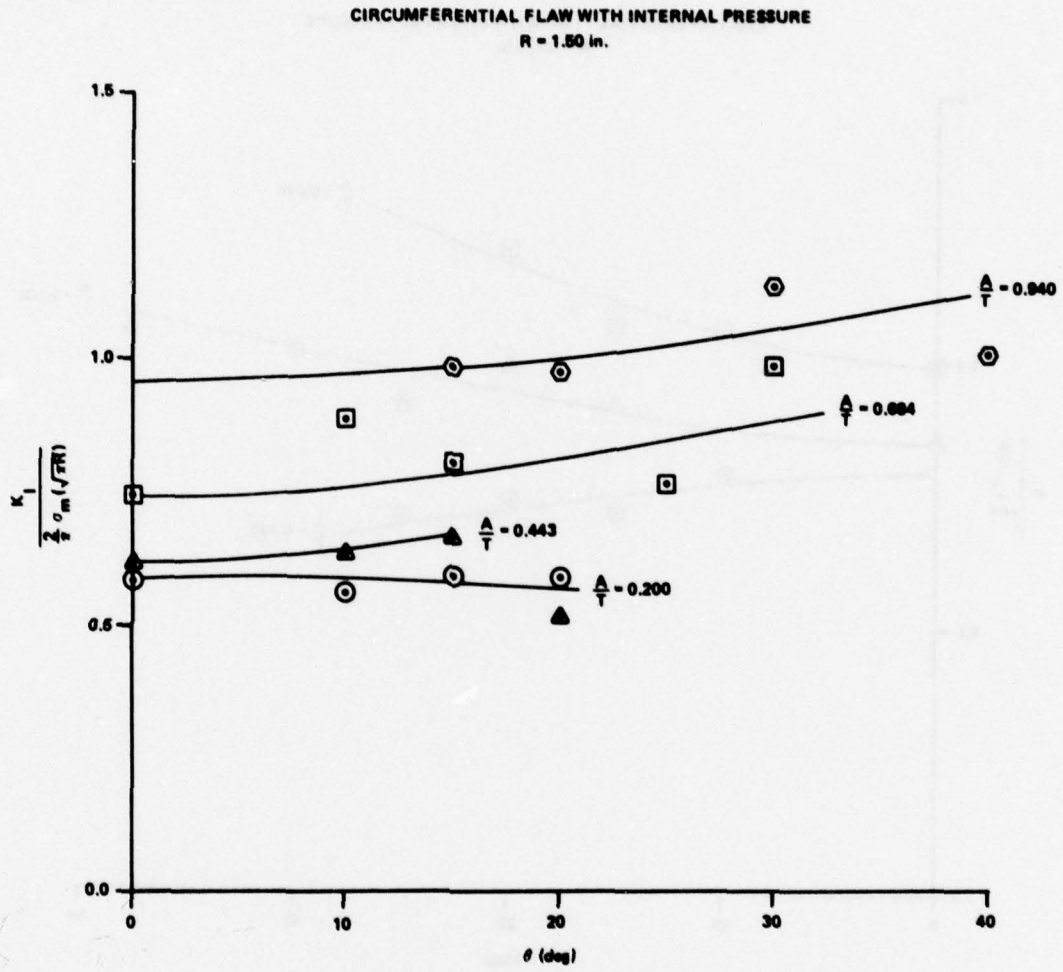

Figure 13. Stress intensity factor versus θ for the transversely-flawed cylinder loaded with internal pressure (R = 1.50 in.).

REFERENCES

1. Mullinix, B. R. and Smith, D. G., An Experimental Determination of the Stress Intensity Around Surface Flaws Embedded in Hollow Cylinders Subjected to Bending, US Army Missile Command, Redstone Arsenal, Alabama, February 1974, Technical Report RL-74-7.

2. Swedlow, J. L., Editor, The Surface Crack: Physical Problems and Computational Solutions, New York: The American Society of Mechanical Engineers, 1972.

3. Smith, D. G. and Mullinix, B. R., Fracture Mechanics Design Handbook, US Army Missile Command, Redstone Arsenal, Alabama, December 1976, Technical Report RL-77-5.

4. Parmerter, R. R., Stress Intensity Factors for Three-Dimensional Problems, Edwards Air Force Base, April 1976, Technical Report RPL-TR-76-30.

5. Smith, C. W., McGowan, J. J., and Peters, W. H., "A Study of Crack-tip Nonlinearities in Frozen Stress Fields," Experimental Mechanics, Vol. 18, No. 8, August 1978.

6. Kassir, M. and Sil, G. C., "Three-Dimensional Stress Distribution Around an Elliptical Crack Under Arbitrary Loading, Journal of Applied Mechanics, Vol. 33, No. 3, September 1966, pp. 601-611.

7. Sneddon, I. N., "The Distribution of Stress in the Neighborhood of a Crack in an Elastic Solid," Proceedings of the Royal Society, Series A, Vol. 187, 1946, pp. 229-260.

8. Thresher, R. W. and Smith, F. W., "Stress-Intensity Factors for a Surface Crack in a Finite Solid, Journal of Applied Mechanics, Series E, Vol. 39, No. 1, March 1972, pp. 195-200.

9. Irwin, G. R., "Discussion of the Dynamic Stress Distribution Surrounding a Running Crack - A Photoelastic Analysis, Proceedings, Society for Experimental Stress Analysis, Vol. 16, No. 1, 1958, pp. 93-96.

Appendix A. TEST DATA

This appendix contains a summary of all the test data presented in this report. The test nomenclature is as follows:

T ≡ Extension loading test, transverse flaw.

PL ≡ Internal pressure loading test, longitudinal flaw

PC ≡ Internal pressure loading test, circumferential flaw (transverse flaw)

The test nomenclature follows the test number. For example, 1PL refers to the first test run of a flaw in the longitudinal orientation subjected to internal pressurization.

Test No. 1T

A/T = 0.206	R = 0.875 in.		σ_m = 10.74 psi
Slice No.	Angle (deg)	K_I	$\frac{K_I}{2/\pi\ \sigma_m\ (\sqrt{\pi R})}$
1	0	7.1788	0.633
2	10	6.0309	0.532
3	15	4.6534	0.410
4	20	4.4673	0.394

Test No. 2T

A/T = 0.390	R = 0.875 in.		σ_m = 10.32 psi
Slice No.	Angle (deg)	K_I	$\frac{K_I}{2/\pi\ \sigma_m\ (\sqrt{\pi R})}$
1	0	10.7465	0.986
2	10	10.6959	0.981
3	15	9.9365	0.912
4	20	9.3772	0.860
5	25	8.7716	0.805

Test No. 3T

A/T = 0.551	R = 0.875 in.		σ_m = 9.72 psi
Slice No.	Angle (deg)	K_I	$\frac{K_I}{2/\pi\ \sigma_m\ (\sqrt{\pi R})}$
1	0	11.9434	1.164
2	15	12.6552	1.233
3	20	11.3063	1.102
4	25	12.4901	1.217
5	30	12.2604	1.195

Test No. 4T

A/T = 0.674	R = 0.875 in.		σ_m = 9.84 psi
Slice No.	Angle (deg)	K_I	$\frac{K_I}{2/\pi\ \sigma_m\ (\sqrt{\pi R})}$
1	0	12.0330	1.158
3	20	14.8617	1.431
4	20	13.7995	1.329
5	30	13.1259	1.264

Test No. 5T

A/T = 0.201	R = 1.50 in.		σ_m = 9.48 psi
Slice No.	Angle (deg)	K_I	$\frac{K_I}{2/\pi\ \sigma_m\ (\sqrt{\pi R})}$
1	0	5.4174	0.413
2	10	5.1066	0.389
3	20	4.0967	0.312

Test No. 6T

A/T = 0.430	R = 1.50 in.		σ_m = 8.416 psi
Slice No.	Angle (deg)	K_I	$\frac{K_I}{2/\pi\ \sigma_m\ (\sqrt{\pi R})}$
1	0	10.5044	0.903
2	10	9.8152	0.844
3	15	8.6668	0.745
4	20	8.5062	0.731
5	25	7.6702	0.659

Test No. 7T

A/T = 0.693	R = 1.50 in.		σ_m = 8.133 psi
Slice No.	Angle (deg)	K_I	$\frac{K_I}{2/\pi\ \sigma_m\ (\sqrt{\pi R})}$
1	0	14.8162	1.318
2	10	14.1479	1.258
3	15	14.2745	1.270
4	25	13.2439	1.178
5	30	13.0841	1.164

Test No. 8T

A/T = 1.10	R = 1.50 in.		σ_m = 5.162 psi
Slice No.	Angle (deg)	K_I	$\frac{K_I}{2/\pi\ \sigma_m\ (\sqrt{\pi R})}$
1	15	16.5615	2.321
2	20	13.6390	1.912
3	30	12.0614	1.691
4	40	11.7697	1.649

Test No. 1PL

A/T = 0.209	R = 0.875 in.		σ_m = 13.138 psi
Slice No.	Angle (deg)	K_I	$\frac{K_I}{2/\pi\ \sigma_m\ (\sqrt{\pi R})}$
1	0	9.7267	0.701
2	10	8.8904	0.641
3	15	10.3859	0.749
4	20	6.0037	0.433
5	25	6.9483	0.501

Test No. 2PL

A/T = 0.388	R = 0.875 in.		σ_m = 11.898 psi
Slice No.	Angle (deg)	K_I	$\frac{K_I}{2/\pi\ \sigma_m\ (\sqrt{\pi R})}$
1	0	11.0324	0.878
2	10	9.7557	0.777
3	15	14.7180	1.172
4	20	12.8083	1.020
5	30	7.7985	0.621
6	35	7.6696	0.611

Test No. 3PL

A/T = 0.553	R = 0.875 in.		σ_m = 10.585 psi
Slice No.	Angle (deg)	K_I	$\frac{K_I}{2/\pi\ \sigma_m\ (\sqrt{\pi R})}$
1	0	14.1988	1.271
2	15	14.9406	1.337
3	20	14.1567	1.267
4	30	13.8462	1.239
5	35	12.2796	1.099

Test No. 4PL

A/T = 0.674	R = 0.875 in.		σ_m = 9.628 psi
Slice No.	Angle (deg)	K_I	$\frac{K_I}{2/\pi\ \sigma_m\ (\sqrt{\pi R})}$
1	0	14.4512	1.422
2	15	13.3491	1.314
3	20	14.3452	1.412
4	30	15.2376	1.499
5	35	15.0910	1.485

Test No. 5PL

A/T = 0.202	R = 1.50 in.		σ_m = 10.474 psi
Slice No.	Angle (deg)	K_I	$\frac{K_I}{2/\pi\ \sigma_m\ (\sqrt{\pi R})}$
1	0	8.4531	0.584
2	5	10.0758	0.696
3	10	8.3307	0.576
4	15	7.7810	0.538
5	20	5.5351	0.382

Test No. 6PL

A/T = 0.448	R = 1.5 in.		σ_m = 9.494 psi
Slice No.	Angle (deg)	K_I	$\frac{K_I}{2/\pi\ \sigma_m\ (\sqrt{\pi R})}$
1	0	10.8909	0.830
2	10	10.9049	0.831
3	15	10.4457	0.796
4	20	10.1675	0.775
5	25	8.5832	0.654
6	30	7.2234	0.551

Test No. 7PL

A/T = 0.580	R = 1.5 in.		σ_m = 8.06 psi
Slice No.	Angle (deg)	K_I	$\frac{K_I}{2/\pi\ \sigma_m\ (\sqrt{\pi R})}$
1	0	14.0269	1.259
2	10	14.2013	1.275
3	15	12.7411	1.144
4	20	15.5208	1.393
5	25	17.2004	1.544
7	35	14.2713	1.281

Test No. 8PL

A/T = 0.868	R = 1.5 in.		σ_m = 6.907 psi
Slice No.	Angle (deg)	K_I	$\frac{K_I}{2/\pi\ \sigma_m\ (\sqrt{\pi R})}$
1	0	16.4216	1.720
2	10	15.6198	1.636
3	15	14.6082	1.530
4	20	14.4427	1.513
5	25	14.4255	1.511
6	30	13.0769	1.370
7	40	13.0989	1.372

Test No. 2PC

A/T = 0.388	R = 0.875 in.		σ_m = 5.93 psi
Slice No.	Angle (deg)	K_I	$\frac{K_I}{2/\pi\ \sigma_m\ (\sqrt{\pi R})}$
2	10	4.9448	0.7899
3	15	4.4775	0.7153
4	20	4.6233	0.7385
5	25	4.3932	0.7018

Test No. 3PC

A/T = 0.531	R = 0.875 in.		σ_m = 5.27 psi
Slice No.	Angle (deg)	K_I	$\frac{K_I}{2/\pi\ \sigma_m\ (\sqrt{\pi R})}$
1	0	4.7515	0.8546
3	15	5.0981	0.9169
4	20	5.4732	0.9844
5	25	5.0620	0.9104
6	30	5.6509	1.0163
7	38	5.8497	1.0521

Test No. 4PC

A/T = 0.674	R = 0.875 in.		σ_m = 9.91 psi
Slice No.	Angle (deg)	K_I	$\frac{K_I}{2/\pi\ \sigma_m\ (\sqrt{\pi R})}$
1	0	10.3759	0.9920
2	10	11.0626	1.0576
3	15	11.1789	1.0687
4	20	12.5803	1.2027

Test No. 5PC

A/T = 0.200	R = 1.500 in.		σ_m = 11.13 psi
Slice No.	Angle (deg)	K_I	$\frac{K_I}{2/\pi\ \sigma_m\ (\sqrt{\pi R})}$
1	0	9.0737	0.5896
2	10	8.6878	0.5645
3	15	9.1832	0.5967
4	20	9.0818	0.5901

Test No. 6PC

A/T = 0.443	R = 1.500 in.		σ_m = 9.92 psi
Slice No.	Angle (deg)	K_I	$\frac{K_I}{2/\pi\ \sigma_m\ (\sqrt{\pi R})}$
1	0	8.4709	0.6179
2	10	8.7018	0.6347
3	15	9.1253	0.6656
4	20	7.0955	0.5175

Test No. 7PC

A/T = 0.684	R = 1.500 in.		σ_m = 8.68 psi
Slice No.	Angle (deg)	K_I	$\frac{K_I}{2/\pi\ \sigma_m\ (\sqrt{\pi R})}$
1	0	8.9268	0.7445
2	10	10.6402	0.8874
3	15	9.6247	0.8027
4	25	9.2004	0.7673
5	30	11.8390	0.9874

Test No. 8PC

A/T = 0.940	R = 1.500 in.		σ_m = 7.54 psi
Slice No.	Angle (deg)	K_I	$\frac{K_I}{2/\pi\ \sigma_m\ (\sqrt{\pi R})}$
1	15	10.2689	0.9845
2	20	10.1580	0.9739
3	30	11.8707	1.1381
4	40	10.4856	1.0053

Appendix B. COMPUTER CODE

The computer code shown on the following pages was used to analyze the photoelasticity data. The code uses the technique presented in Section IV with a least squares straight-line curve fit of the experimental data.

```
C -----PHOTOELASTICITY CODE-CYLINDERS
      DIMENSION AN(50),AR(50),AT(50),AK(50),ID(50)
      WRITE(5,22)
22    FORMAT(' NO. OF SLICES?')
      READ(5,1) N
1     FORMAT(I3)
      DO 19 I=1,N,1
      WRITE(5,2)
2     FORMAT(' NO. OF DATA POINTS?')
      READ(5,1) M
      WRITE(5,23)
23    FORMAT(' FRINGE CONSTANT?')
      READ(5,24) F
24    FORMAT(F10.0)
      WRITE(5,25)
25    FORMAT(' SLICE THICKNESS?')
      READ(5,26) T
26    FORMAT(F10.0)
      WRITE(5,27)
27    FORMAT(' INPUT R AND N-F4.0,F6.0:')
      DO 4 J=1,M,1
      READ(5,3) AR(J),AN(J)
3     FORMAT(F4.0,F6.0)
4     CONTINUE
      AMAX=0.
      DO 5 J=1,M,1
      AT(J)=F*AN(J)/(2.*T)
      AK(J)=AT(J)*SQRT(8.*3.14159*AR(J))
      IF(AK(J).GT.AMAX) AMAX=AK(J).
5     AR(J)=SQRT(AR(J))
6     CALL IPOKE("170410,"1)
      CALL IPOKE("170410,"0)
      DO 7 J=1,M,1
      IY=INT(AK(J)*1000./AMAX)
      IX=INT(AR(J)*1000./AR(M))
      CALL IPOKE("170412,IX)
      CALL IPOKE("170414,IY)
7     CALL IPOKE("170414,"0)
      ITEST=IPEEK("177570)
      IF(ITEST.EQ.0) GOTO 6
      WRITE(5,8)
```

```
8       FORMAT(' NO. OF DELETE SAMPLES?')
        READ(5,9) ND
9       FORMAT(I3)
        IF(ND.EQ.0) GOTO 20
        DO 11 J=1,ND,1
        READ(5,10) ID(J)
10      FORMAT(I3)
11      CONTINUE
20      CONTINUE
        X1=0.
        X2=0.
        Y0=0.
        Y1=0.
        DO 14 J=1,M,1
        IF(ND.EQ.0) GOTO 21
        DO 13 K=1,ND,1
13      IF(J.EQ.ID(K)) GOTO 14
21      X1=X1+AR(J)
        X2=X2+AR(J)**2.
        Y0=Y0+AK(J)
        Y1=Y1+AK(J)*AR(J)
14      CONTINUE
        AK1=(X2*Y0-Y1*X1)/(FLOAT(M-ND)*X2-X1*X1)
        WRITE(5,15) I
15      FORMAT(' SLICE NO.=',I3)
        DO 18 J=1,M,1
        AR(J)=AR(J)**2.
        WRITE(5,16) AR(J),AN(J),AT(J),AK(J)
16      FORMAT(' R=',F10.4,5X,'N='F10.4,5X,
       1'TMAX=',F10.4,5X,'KAPP='F10.4)
18      CONTINUE
        WRITE(5,17) AK1
17      FORMAT(' K1=',F14.4)
19      CONTINUE
        STOP
        END
*
```

DISTRIBUTION

	No. of Copies
Headquarters SAC/NRI (Stinfo Library) Offutt Air Force Base, Nebraska 68113	1
Commander (Code 233) Naval Weapons Center Attn: Library Division China Lake, California 93555	1
Department of the Army US Army Research Office Attn: Information Processing Office P. O. Box 12211 Research Triangle Park, North Carolina 27709	1
ADTC (DLDSL) Eglin Air Force Base, Florida 32542	1
University of California Los Alamos Scientific Laboratory Attn: Reports Library P. O. Box 1663 Los Alamos, New Mexico 87545	1
Library US Army War College Carlisle Barracks, Pensylvania 17013	1
Tennessee Technological Univeristy Department of Engineering Science Attn: Dallas G. Smith Cookeville, Tennessee 38501	1
Defense Documentation Center Cameron Station Alexandria, Virginia 22314	12
Defense Metals Information Center Battelle Memorial Institute 505 King Avenue Columbus, Ohio 43201	1
Commander US Army Foreign Science and Technology Center Attn: DRXST-SD3 220 Seventh Street, NE Charlottesville, Virginia 22901	1
Office of Chief of Research and Development Department of the Army Attn: DARD-ARS-P Washington, D. C. 20301	1
Commander US Army Natick Laboratories Kansas Street Attn: STSNLT-EQR Natick, Massachusetts 01760	1
Commander US Army Mobility Equipment Research and Development Center Fort Belvoir, Virginia 22060	1
Commander Edgewood Arsenal Attn: SAREA-TS-A Aberdeen Proving Ground, Maryland 21010	1
Commander Picatinny Arsenal Attn: SARPA-TS-S, Mr. M. Costello Dover, New Jersey 07801	1
Commander Watervliet Arsenal Watervliet, New York 12189	1
Commander US Army Test and Evaluation Command Attn: DRSTE-RA Aberdeen Proving Ground, Maryland 21005	1
Director Air Force Materiel Laboratory Attn: AFML-DO-Library Wright-Patterson AFB, Ohio 45433	1
Director, Army Materials and Mechanics Research Center Attn: DRXMR-PL -MT, Mr. Farrow Watertown, Massachusetts 02172	1 1
Technical Library Naval Ordnance Station Indian Head, Maryland 20640	1
Commander US Army Materiel Development and Readiness Command Attn: DRCMT Washington, D. C. 20315	1
US Army Research and Standardization Group (Europe) Attn: DRXSN-E-RX, Dr. Alfred K. Nedoluha Box 65 FPO New York 09510	2
US Army Materiel Development and Readiness Command Attn: Mr. Edward Sedlak Dr. James Bender 5001 Eisenhower Avenue Alexandria, Virginia 22333	1 1
Headquarters, Department of the Army Office of the Deputy Chief of Staff for Research and Development and Acquisition Attn: DAMA-ARZ Room 3A474, Pentagon Washington, D. C. 20310	2
Director Defense Research and Engineering Attn: Mr. Leonard R. Weisberg Room 3D1079, Pentagon Washington, D. C. 20301	2
Director Defense Advanced Research Projects Agency 1400 Wilson Boulevard Arlington, Virginia 22209	1
Commander US Army Research Office Attn: DRXRO-PH, Dr. R. Lontz P. O. Box 12211 Research Triangle Park, North Carolina 27709	2
Southern Technologies, Inc. Attn: T. Ward 1013 Meridian Street North Huntsville, Alabama 35801	1
DRSMI-LP, Mr. Voigt	1
DRDMI-X, Mr. McKinley	1
-T, Dr. Kobler	1
-TL, Mr. Lewis	1
-TLA, Mr. Pettey	1
Mr. Schaeffel	50
-TBD	3
-TI (Record Set)	1
(Reference Copy)	1

☆U.S. GOVERNMENT PRINTING OFFICE: 1979—640-122/325